Journal of Mechatronics, Electrical Power, and Vehicular Technology 16 (2025) 185-203

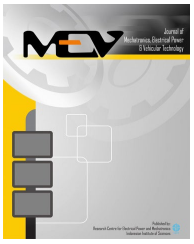

Journal of Mechatronics, Electrical Power, and Vehicular Technology

e-ISSN: 2088-6985
p-ISSN: 2087-3379

mev.brin.go.id

Enhanced outdoor localization of low-cost personal mobility vehicles using Extended Kalman Filter sensor fusion

Vita Susanti [a, b], Mohd Saiful Azimi Mahmud [a, *], Roni Permana Saputra [b]

[a] *Faculty of Electrical Engineering, Universiti Teknologi Malaysia Skudai*
School of Electrical Engineering, Faculty of Engineering, Universiti Teknologi Malaysia, 81310 UTM Skudai, Johor, Malaysia
[b] *Research Center for Smart Mechatronics, National Research and Innovation Agency (BRIN)*
Kawasan Sains dan Teknologi (KST) Samaun Samadikun, Jalan Sangkuriang, Bandung, 40135, Indonesia

Abstract

Personal mobility vehicles (PMVs) are gaining popularity for short urban trips, reducing car reliance and urban pollution. The development of autonomous PMVs heavily relies on accurate localization, often using the global positioning system (GPS) as a primary sensor. However, standard GPS suffers from poor accuracy, which requires data fusion with supplementary sensors to improve precision. This study presents a sensor fusion approach using low-cost, consumer-grade hardware to enhance the PMV localization. The fusion system integrates data from an inertial measurement unit (IMU) and wheel odometry with GPS, fusing them via Kalman Filter (KF) and Extended Kalman Filter (EKF) methods. A field experiment was conducted along a 67-meter route at velocities ranging from 0.25 to 1.23 m/s. Comparative analysis has shown that the EKF method consistently outperforms the standard KF, improving positioning accuracy by approximately 29 % and reducing the maximum deviation to a range of 1.8 m to 2.7 m across different velocities. The results have confirmed the EKF as an effective and reliable strategy for achieving high-precision localization with affordable sensors, a key step towards scalable autonomous navigation for PMVs.

Keywords: Extended Kalman Filter; sensor fusion; low-cost sensors; personal mobility vehicles; autonomous navigation; outdoor navigation; outdoor localization; localization accuracy.

I. Introduction

In recent years, there have been significant advancements in transportation technology, which have been driven by the need for mobility solutions that are more efficient, sustainable, and accessible. Personal mobility vehicles (PMVs), which include electric wheelchairs, scooters, and electric bikes, have gained more popularity recently as efficient, sustainable, and accessible transportation options for daily mobility and assisted living [1].

To further improve the functionality of these vehicles, one promising strategy is the integration of autonomous features. This integration aims to provide more convenient, efficient, and comfortable operation for the users. Autonomous PMVs can navigate through complex environments and avoid obstacles without continuous human intervention [2][3]. This capability depends on the precise and reliable navigation systems that can accurately determine the vehicle's position and orientation in real-time, a requirement that is particularly critical in varied outdoor environments [4].

* Corresponding Author. azmi@utm.my (M. S. A. Mahmud)

https://doi.org/10.55981/j.mev.2025.1294

Received 21 August 2025; revised 23 September 2025; accepted 26 September 2025; available online 23 December 2025; published 31 December 2025

How to Cite: V. Susanti *et al.*, "Enhanced outdoor localization of low-cost personal mobility vehicles using Extended Kalman Filter sensor fusion," *Journal of Mechatronics, Electrical Power, and Vehicular Technology*, vol. 16, no. 2, pp. 185-203, Dec., 2025.

However, achieving reliable autonomy in cost-sensitive PMVs is primarily hindered by the limitations of affordable positioning systems, particularly in challenging urban environments.

In outdoor navigation, the global positioning system (GPS) is commonly used as a primary sensor. However, its performance can be greatly affected by signal loss, multipath effects, and reduced accuracy in densely populated urban regions [5][6][7]. These limitations will create a significant challenge for safe autonomous operation, which requires an accurate representation of the environment and a reliable assessment of the vehicle's current state, a process known as localization.

To address these challenges, sensor fusion methods are commonly used to combine data from multiple sources [8]. These methods leverage the complementary strengths of different sensors to mitigate the weaknesses of any individual one, providing more robust and accurate localization results [9]. Sensor fusion often involves augmenting GPS with additional sensors such as an odometer, which is known for its short-term accuracy and robust resistance to external interference, and an inertial measurement unit (IMU), which provides crucial data on acceleration and rotation. When these sensors are fused with GPS through an integrated navigation system (INS), the positional accuracy and reliability will be significantly enhanced [10].

In addition, other sensors such as light detection and ranging (LiDAR), radar, and magnetometers are also frequently integrated in navigation systems to create a more comprehensive perception of the environment [11][12]. The data fusion can be implemented at three levels, which are low-level (raw data), mid-level (feature), and high-level (decision-making) [13]. The integrated data from these sensors will create a critical foundation for the vehicle's decision-making processes.

Several methods have been designed in sensor fusion to improve the precision of the GPS-based localization system. Among these, the Extended Kalman filter (EKF) has been widely investigated for its effectiveness in combining various sensor data with the GPS localization system. For instance, the EKF method can enhance vehicle position estimation accuracy by predicting position and velocity data based on IMU and odometry inputs and subsequently updating this information using GPS data, thereby guaranteeing long-term accuracy [14][15][16].

The EKF offers several benefits, including the ability to precisely track the GPS data for position and velocity estimates, demonstrating its strong implementation potential [9][15][16]. Other advantages include its local stability, ease of implementation, and relatively low computational cost, making it suitable for real-time applications on constrained hardware [17]. The EKF works well for estimating nonlinear states [18], processing noisy measurements in dynamic systems in real-time [19] and estimating vehicle state parameters with high accuracy [20].

However, EKF's performance is dependent on the quality of its models and sensors, where the use of low-cost components can impact data reliability. In addition, incorrect system modeling or noise characteristics can also significantly reduce the EKF's effectiveness. Although EKF-based sensor fusion is a well-established sensor fusion method in automotive and high-precision robotics applications, its implementation for low-cost PMVs introduces unique challenges. These challenges arise from the use of consumer-grade sensors and the distinctive dynamic profile characteristic of low-speed vehicles, an area that has received comparatively limited attention in existing literature.

Several studies have utilized the low-cost global navigation satellite system (GNSS), IMU, odometry, and the sensor fusion has been conducted using a Kalman Filter-based method. However, the approach proposed in [21] was constrained by its limited applicability in the x and y dimensions; thus, it is found to be not compatible for hill terrains, and it also employs a basic EKF model without any dynamic noise adaptation [21]. Other studies employ GPS and IMU using the Unscented Kalman Filter (UKF) methodology, utilizing the KITTI dataset. However, this research exhibits significant computing complexity and is susceptible to error modelling [22]. Study in [23] offered an asynchronous integration of GPS, IMU, and controller area network (CAN) bus odometry using EKF, which effectively manages asynchronous data, but it is found to be less appropriate for real-time applications because of its processing demands and non-causal characteristics [23]. In the study of [24], the integration of GPS, IMU, and odometer with EKF demonstrates greater stability under GPS disturbances. Nonetheless, it still encounters cumulative errors upon the loss of previous GPS data and is constrained to basic test scenarios [24]. Therefore, this study investigates the implementation of an EKF-based sensor fusion system to enhance the outdoor navigation capabilities of cost-effective PMV. By integrating data from consumer-grade GPS, wheel odometry, and an IMU, the study aims to improve the accuracy and reliability of vehicle localization in challenging outdoor environments. Therefore, the main objective of this work is to design an advanced, yet accessible navigation technology that is both practical and applicable for real-life scenarios.

More specifically, the contributions of this study include:

1. Design and development of a practical EKF-based fusion algorithm for cost-effective PMVs: the study presents a sensor fusion architecture based on the EKF, designed for cost-effective personal mobility vehicles (PMVs). This approach provides a practical and effective method to enhance the precision and reliability of outdoor navigation systems that would otherwise be compromised by low-cost GPS.
2. Comprehensive experimental validation: the research includes extensive experimental validation in real-world outdoor settings. These experiments evaluate the system's performance, demonstrating not only its feasibility but also a significant improvement in localization accuracy and reliability.
3. Enhancing accessibility through advanced affordable navigation technology: the research emphasizes cost-effective solutions by using consumer-grade GPS sensors with low-cost complementary sensors, making advanced navigation technologies more accessible for real-world applications and commercial viability.

The remainder of this paper is organized as follows: Section 1 reviews related research on sensor fusion methods, localization methods for autonomous systems, and the specific application of the EKF in robotics and autonomous vehicles. Section 2 details the materials and methods, encompassing the vehicle system, the integration of sensors (GPS, IMU, and wheel encoders), the experimental setup (including environments, PMV configuration, and data collection process), the design and implementation of the EKF-based sensor fusion algorithm, and the evaluation criteria for the proposed system. Section 3 analyzes the experimental results, comparing the proposed method with baseline GPS localization methods and discussing improvements in accuracy. Finally, Section 4 summarizes the key findings, highlights the importance of EKF-based sensor fusion in PMV navigation, and suggests potential pathways for future research.

II. Materials and Methods

A. Personal mobility vehicle

A personal mobility vehicle (PMV) is a type of electric vehicle that is becoming increasingly popular [25]. These vehicles, powered by an electric motor, can reach velocities of about 2 m/s, which is comparable to the walking velocity of an average person [26][27]. PMVs are primarily used in urban settings or restricted areas for short-distance travel ranging from 0.8 to 3.2 km, with the aim of minimizing car usage for short distances [25]. In many European cities, PMVs are more popular than bicycles. Figure 1 illustrates the categorization of PMVs according to their velocity. This study utilized a low-velocity PMV in its framework.

B. SEATER: Single passenger electric autonomous transporter

Introduced in 2023, the National Research and Innovation Agency (BRIN) developed the SEATER as a new type of PMV. The design allows it to operate autonomously in specific and controlled spaces like airports, theme parks, large office buildings, and similar indoor areas. Its purpose is to offer a safe and convenient mode of transportation within these environments. Although it is still in the development phase, SEATER has the potential to transform personal transportation, making urban areas more livable and sustainable in the future.

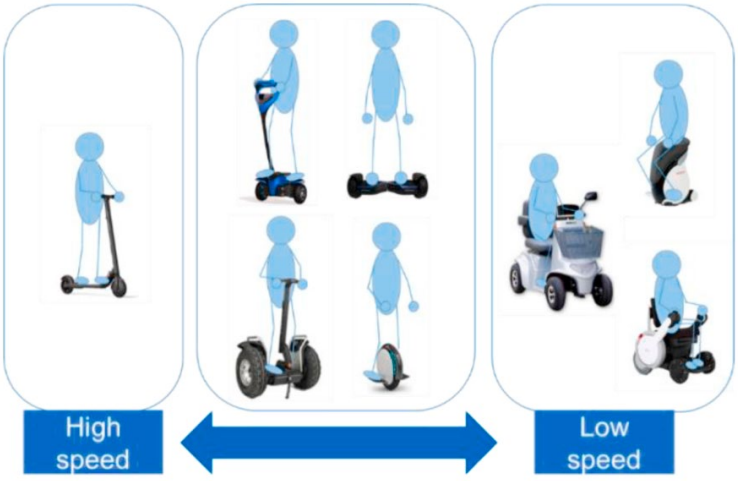

Figure 1. PMVs categories (adopted from [28]).

Figure 2. The SEATER.

Figure 2 illustrates components present on the SEATER, including features and sensors. Additionally, there is a joystick available for manual operation. Several sensors are present, including a camera, GPS, odometry, and IMU (positioned beneath the seat). There are two types of wheels: the rear wheels are differential wheel drives, and the front wheels are omnidirectional supporting wheels [29]. Table 1 provides the specifications for the SEATER platform, a compact personal mobility vehicle that is ideal for confined spaces usage where agility is crucial, such as indoor environments or heavily crowded urban regions.

C. Sensor integration

The experiment platform incorporates GlobalSat BU-353N5 GPS, Adafruit BNO055 9-DOF IMU, and wheel odometry sensors that function as navigation sensors. The PMV mounts the GPS sensor on its arm, places the IMU under its seat, and places the wheel odometry on its rear wheels. The GPS sensor provides absolute position data used as the main reference for navigation. The IMU sensor provides orientation and motion data that help improve the vehicle's position and orientation when the GPS signal is unavailable or disrupted, as well as detect changes in direction and velocity. Meanwhile, the wheel odometry sensor accurately measures the vehicle's distance traveled and velocity. The GPS and IMU refine their position estimates using this data, particularly when the GPS data is inaccurate. All this sensor data is processed using the Kalman Filter and the Extended Kalman Filter method.

Table 1.
SEATER specification.

Specification	Description
Type	Autonomous personal mobility vehicle
Driving type	Electric drive; differential drive
Dimension	Approx. 120x75x110 cm
Weight	Approx. 50 kg
Passenger capacity/maximum weight	1 person/max 120 kg
Max velocity	1.5 m/s or approx. 5 km/hour
Max coverage distance	Approx. 10 km
Max operational duration (fully charged)	Approx. 2 hours
Operational mode	Manual/autonomous

D. Environmental setting

Figure 3 shows the data collection site, which is located at KST Samaun Samadikun, BRIN, Bandung (-6.8820317˚, 107.6114834˚). The yellow line illustrates the path followed by SEATER, starting at point A and ending at point B. The total track length is approximately 67 meters.

E. Data collection procedure

Figure 4 shows the data collection process and extraction for SEATER. In this study, the data collection process was repeated three times for each variation of velocity to verify the accuracy of the collected data and to facilitate cross-set comparisons. Additionally, it helps to observe the patterns of the data.

The data collection path was 67 meters long, and the SEATER moved at a constant velocity as predetermined, ensuring consistent data since the velocity variable did not change during data collection.

Figure 4 illustrates the data collection procedure conducted across five different velocity levels, with each velocity level repeated three times to ensure data reliability. Data from the GPS, IMU, and odometry

Figure 3. Path used for data collection.

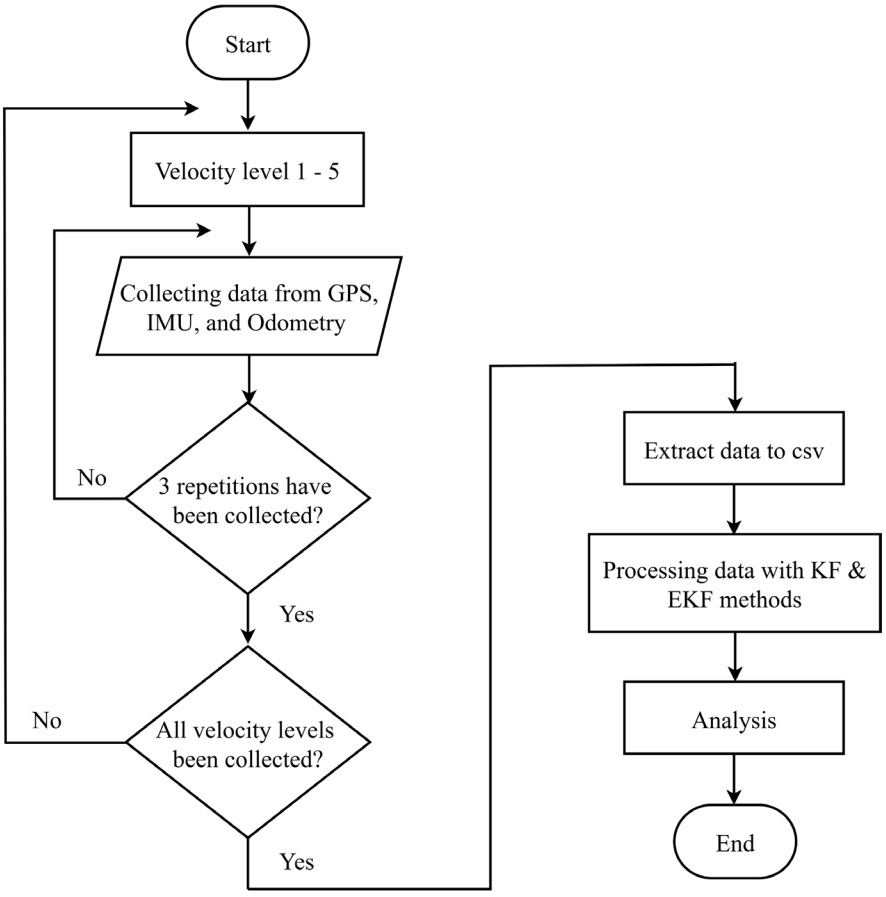

Figure 4. Data collection procedure.

Table 2.
Variation of velocity level.

Velocity Level	Velocity
Velocity 1	0.5 m/s
Velocity 2	0.7 m/s
Velocity 3	0.9 m/s
Velocity 4	1 m/s
Velocity 5	1.23 m/s

sensors were collected at each velocity level and extracted into a CSV file for further analysis. Following data collection, Kalman Filter and Extended Kalman Filter methods were designed to fuse the localization data, and the localization accuracy achieved by each approach was analyzed.

Table 2 displays the velocity variations and their corresponding velocity level. Three trials were conducted for each velocity level in the experiment to gather robust data. Table 3 presents the quantitative measure of the total data collected. The data obtained from the GPS sensor are captured at a frequency of 1 Hz (one data point per second), while the IMU data were captured approximately 100 Hz (100 data points per second), and the odometry data were captured at over 200 Hz (more than 200 data points every second). The SEATER's velocity influences the duration of each trial: higher velocity shortens travel time, resulting in less data collected, while lower velocity extends travel time, allowing for a greater volume of data to be collected.

F. Evaluation criteria

This study employs a metric-based approach to evaluate the enhancement in localization precision achieved by the Kalman Filter (KF) and Extended Kalman Filter (EKF) algorithms. The study compares the estimated vehicle positions from the KF and EKF against the raw GPS measurements. The primary objective is to quantify the reduction in positional error (deviation) offered by the filtered estimates, thereby assessing their effectiveness and optimization in improving GPS accuracy.

The key metric for this assessment is the Euclidean distance between the estimated position from the filter (the best estimate of the true position) and the raw GPS measurement. This deviation, calculated for each data point, provides a direct measure of the filter's correction. A smaller deviation indicates a more significant correction and a higher improvement in accuracy. The overall performance is then evaluated by analyzing the statistical distribution (e.g., mean, maximum, standard deviation) of these errors across the entire dataset.

Localization performance was assessed using a metric-based approach centered on lateral deviation (Dev), defined as the signed perpendicular distance from an estimated position to a straight-line reference path. Let the reference path be the line segment from the start point $P_0 = (x_0, y_0)$ to the goal $P_f = (x_f, y_f)$ where x_0 and y_0 is the initial coordinate and x_f and y_f is the final coordinate, respectively. The nominal path heading is defined in equation (1) as:

Table 3.
Data collection for each variation of velocity level.

Velocity variation		Number of data		
		GPS	IMU	Odometry
Velocity 1	Exp 1	137	13735	27471
	Exp 2	131	13090	26179
	Exp 3	135	13479	26954
Velocity 2	Exp 1	95	9518	19019
	Exp 2	97	9655	19318
	Exp 3	94	9386	18775
Velocity 3	Exp 1	70	7060	14592
	Exp 2	72	7214	14423
	Exp 3	73	7301	14592
Velocity 4	Exp 1	63	6231	12460
	Exp 2	74	7364	14731
	Exp 3	61	6134	12265
Velocity 5	Exp 1	53	5310	10621
	Exp 2	52	5237	10472
	Exp 3	54	5412	10814

$$\theta_{ref} = atan2(y_f - y_0, x_f - x_0) \quad (1)$$

For any estimated position $P = (x, y)$ (from GPS, KF, or EKF), the expected y-coordinate on the reference path at the same x-coordinate is defined as equation (2):

$$y_{act} = y_0 + tan(\theta_{ref})(x - x_0) \quad (2)$$

and the instantaneous Dev is given as equation (3):

$$\text{Dev} = y - y_{act} \quad (3)$$

where smaller $|Dev|$ indicates closer adherence to the intended trajectory. For each trajectory $\{\text{Dev}_k\}_{k=1}^{N}$, it can be seen in equation (4) and equation (5) that:

$$\text{Max Dev} = \max_k |Dev_k| \quad (4)$$

$$\sigma_{\text{Dev}} = \sqrt{\frac{1}{N-1}\sum_{k=1}^{N}(\text{Dev}_k - \mu_{\text{Dev}})} \quad (5)$$

Here, μ_{Dev} reflects average signed bias, Max Dev captures worst-case lateral error, and σ_{Dev} is the Standard Dev indicating consistency/stability.

G. Extended Kalman Filter architecture

The Kalman Filter (KF) is a prediction/update method that generates optimal estimation on unknown variables by using a sequence of measurements recorded over time, which may contain statistical noise. Based on Bayesian probability, this method computes optimal estimates by utilizing Gaussian probability distributions and linear algebra [30].

In contrast, the Extended Kalman Filter (EKF) is utilized for nonlinear systems [21]. EKF manages nonlinearity by linearizing the system around the current estimate point, which is subsequently processed via the Kalman Filter [31]. Nonlinearity in a problem can manifest in two key areas: the process model employed for state prediction and the measures derived from the observation model.

In the experiment, the variables used in the state vector are shown in equation (6), where x_k is the state vector, x and y are the position from the GPS sensor, ψ is heading from IMU, v is velocity from odometry, and $\dot{\psi}$ is the yaw rate from IMU.

$$x_k = \begin{bmatrix} x \\ y \\ \psi \\ v \\ \dot{\psi} \end{bmatrix} = \begin{bmatrix} Position\ X \\ Position\ Y \\ Heading \\ Velocity \\ Yaw\ rate \end{bmatrix} \quad (6)$$

Figure 5 illustrates the Extended Kalman Filter cycle, highlighting the role of the Jacobian matrix, which represents the partial derivatives of the nonlinear function with respect to its variables. The Jacobian matrix is essential for linearizing the nonlinear model, allowing the filter to estimate the state of the nonlinear system. The Jacobian matrix is critical in EKF, as it helps to deal with the system's nonlinearity and measurements. By linearizing the model via the

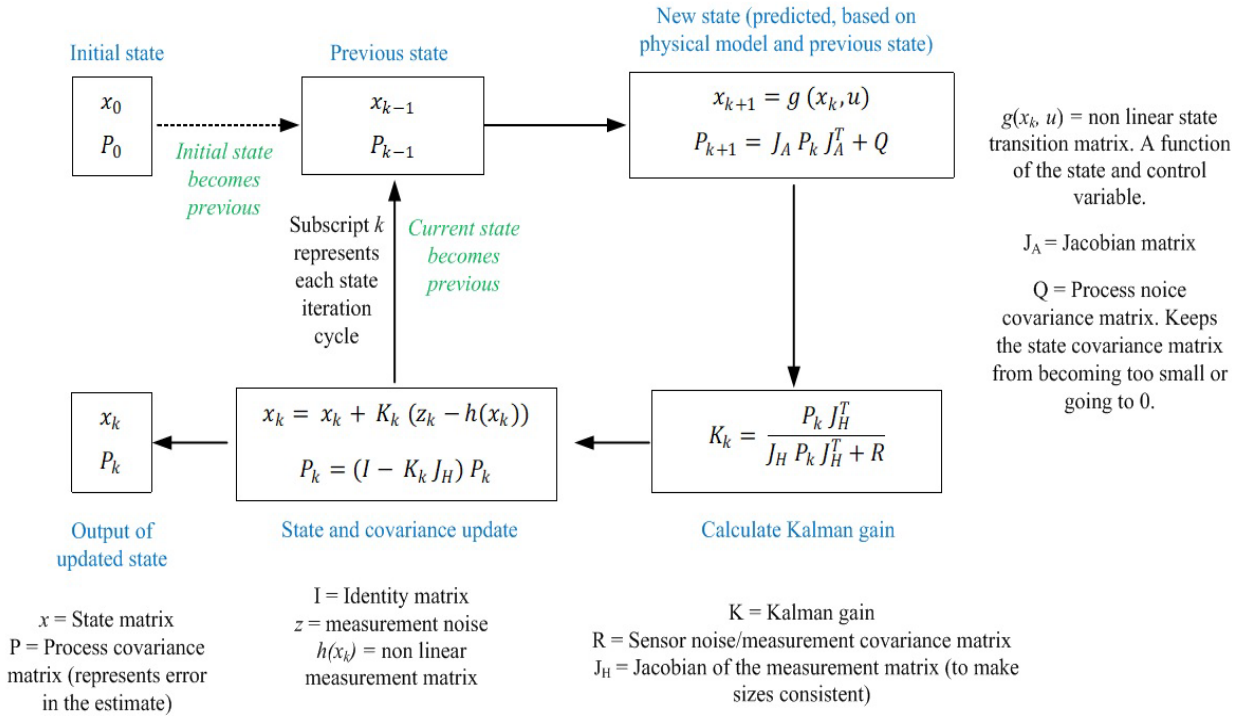

Figure 5. Extended Kalman Filter system [32].

Jacobian matrix, EKF can work with nonlinear models and provide better estimates of the system's state.

The EKF cycle starts with an initial state estimate $\mathbf{x}_0$ and covariance $\mathbf{P}_0$. In the prediction phase, the current estimate is propagated through the nonlinear motion model $g(\cdot)$. Since the model is nonlinear, it is then locally linearized with the state Jacobian, $\mathbf{J}_A = \partial \mathbf{g}/\partial \mathbf{x}$. When a sensor reading arrives, the update phase is executed by comparing the measurement with the predicted measurement from the nonlinear sensor measurement model $\mathbf{h}(\cdot)$, linearized by the measurement Jacobian $\mathbf{J}_H = \partial \mathbf{h}/\partial \mathbf{x}$. Kalman gain then balances trust between model and sensor to produce a corrected state and reduced covariance. The corrected pair becomes the starting point for the next cycle (and multiple updates can occur asynchronously within one time step). The complete EKF formulation is provided in equation (7) to equation (13).

Prediction:

$$\mathbf{x}_k = \boldsymbol{g}(\mathbf{x}_{k-1}, \mathbf{u}_k) \tag{7}$$

$$\mathbf{P}_k = \mathbf{J}_A \, \mathbf{P}_{k-1} \, \mathbf{J}_A^T + \boldsymbol{Q} \tag{8}$$

Update:

$$\tilde{\mathbf{y}}_k = \mathbf{z}_k - \mathbf{h}(\mathbf{x}_k) \tag{9}$$

$$\mathbf{S}_k = \mathbf{J}_H \, \mathbf{P}_k \, \mathbf{J}_H^T + \mathbf{R} \tag{10}$$

$$\mathbf{K}_k = \mathbf{P}_k \, \mathbf{J}_H^T \, \mathbf{S}_k^{-1} \tag{11}$$

$$\mathbf{x}_k = \mathbf{x}_k + \mathbf{K}_k \tilde{\mathbf{y}}_k \tag{12}$$

$$\mathbf{P}_k = (\mathbf{I} - \mathbf{K}_k \mathbf{J}_H)\mathbf{P}_k \tag{13}$$

The process-noise covariance is denoted by $\mathbf{Q}$ (capturing unmodeled dynamics), and the measurement-noise covariance by $\mathbf{R}$ (capturing sensor uncertainty).

H. Implementation setting of the EKF method

The EKF extends the linear Kalman Filter to nonlinear systems by linearizing the process and measurement models around the current state estimate. The implementation assumes a planar (2D) motion model for a ground vehicle, estimating position, velocity, and heading on a flat surface. The algorithm operates through a continuous cycle of prediction and update steps, fusing asynchronous data from multiple sensors. The overall workflow of this iterative process is illustrated in Figure 6.

As shown in Figure 6, the process begins with the initialization of the state vector and covariance matrix $(\mathbf{x}_0, \mathbf{P}_0)$. The algorithm then iterates through a prediction step, where the next state $(\mathbf{x}')$ and its covariance $(\mathbf{P}')$ are projected using the motion model, and an update step, where new sensor data is fused to correct the prediction. The Kalman Gain $(\mathbf{K})$ is computed to optimally balance the weight given to the new measurements against the prior predictions. This gain is then used to update the state estimate $(\mathbf{x})$, refining the position, velocity, and orientation estimates. The covariance estimate $(\mathbf{P})$ is also updated to reflect the reduced uncertainty. The cycle then repeats, ready for the next iteration.

1) Process and measurement model definition

The EKF operates on two fundamental models: the process model, which predicts the evolution of the state, and the measurement model, which predicts the sensor outputs based on the state.

The discrete-time process model is defined as equation (14).

$$\mathbf{x}_k = f(\mathbf{x}_{k-1}, \mathbf{u}_{k-1}) + \mathbf{w}_{k-1} \tag{14}$$

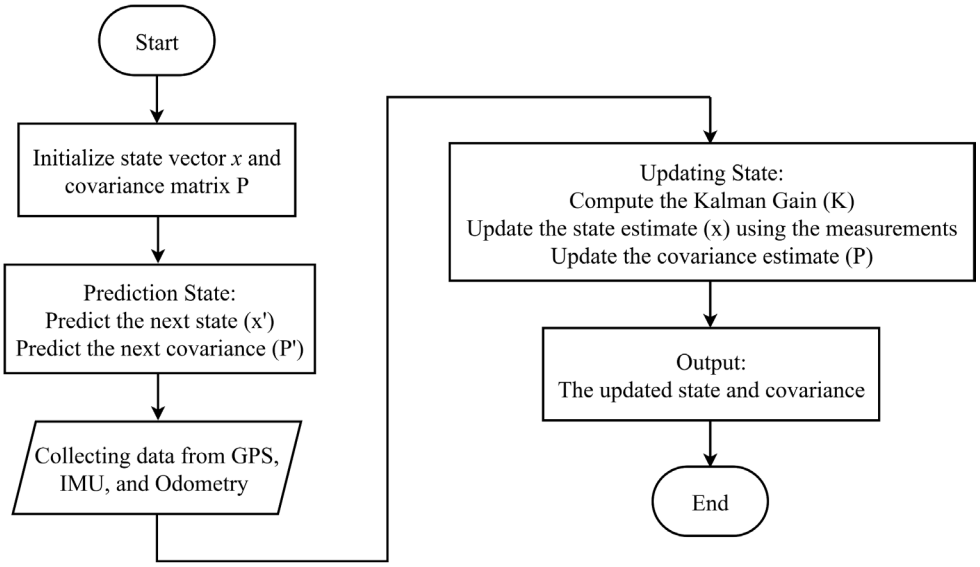

Figure 6. EKF flowchart. The filter initializes $(\mathbf{x}_0, \mathbf{P}_0)$, predicts $(\mathbf{x}', \mathbf{P}')$ using the motion model and process noise $\mathbf{Q}$, then updates on measurement arrival by computing the Kalman gain, correcting the state and covariance, and repeating.

where $\mathbf{x}_k$ is the state vector at time step k, $f(\cdot)$ is the nonlinear state transition function, $\mathbf{u}_{k-1}$ is the control input, and $\mathbf{w}_{k-1}$ is the process noise, assumed to be zero-mean Gaussian with covariance $\mathbf{Q}$.

For the planar implementation, the state vector is simplified to $\mathbf{x} = [px, py, \psi, v, \psi]^{\mathrm{T}}$ (see equation 6) where (px, py) represent the 2D position in the world frame; ψ is the vehicle's heading (yaw) angle; v represents the linear velocity (speed); and $\dot{\psi}$ is the yaw rate. A constant turn rate and velocity (CTRV) model was employed. The control input $\mathbf{u}$ is derived from the inertial measurement unit (IMU) gyroscope for yaw rate and wheel odometry for velocity.

The measurement model is defined as equation (15).

$$\mathbf{z}_k = \mathrm{h}(\mathbf{x}_k) + \mathbf{v}_k \tag{15}$$

where $\mathrm{h}(\cdot)$ maps the state to the expected measurement, and $\mathbf{v}_k$ is the measurement noise with covariance $\mathbf{R}$.

A loosely coupled strategy was adopted for its simplicity and robustness. This approach fuses the navigation outputs (e.g., position, velocity) from various sensors rather than raw measurements. The system is asynchronous, and the fusion framework performs a state update whenever a measurement from any sensor arrives.

2) EKF covariances and tuning

The initial state covariance (P) is formulated as equation (16).

$$\mathbf{P}_0 = diag(\sigma_p^2, \sigma_p^2, \sigma_\psi^2, \sigma_v^2, \sigma_{\dot{\psi}}^2) \tag{16}$$

with large diagonal entries reflecting prior uncertainty. The process noise $\mathbf{Q}$ captures CTRV model mismatch (e.g., unmodeled longitudinal/lateral accelerations and turn-rate perturbations) and is tuned empirically to balance responsiveness and noise attenuation. The Measurement Noise Covariance $\mathbf{R}$ is represented as a diagonal matrix in equation (17).

$$\mathbf{R} = \begin{bmatrix} R_{GPS} & 0 \\ 0 & R_{GPS} \end{bmatrix} \tag{17}$$

Initialized from sensor datasheets and refined manually along the process.

3) Sensor synchronization

The sensors used in the experiments operate at different rates (e.g., IMU: 50 Hz, GPS: 10 Hz, Odometry: 100 Hz). To enable consistent fusion across disparate sampling rates, the following procedures are employed:

a) Hardware Timestamping: All sensor data was tagged with a common timestamp upon arrival.
b) Rate alignment (prediction vs. update): The EKF prediction executes at the highest available rate (100 Hz). Updates are performed at each measurement's exact timestamp; slower sources (e.g., GPS) are not upsampled and update only at their native rate to avoid phase lag. When necessary, the predicted state is propagated to the precise measurement time prior to correction.

4) Calibration procedures

The Bosch BNO055 IMU performs on-board, automatic calibration of the magnetometer, gyroscope, and accelerometer. Following calibration, the device provides bias-compensated, low-pass–filtered measurements; calibration status flags were continuously monitored, and measurements were admitted to the fusion pipeline only when the sensor reported a fully calibrated state. The BU-353N5 GPS receiver requires no user-initiated calibration, as signal conditioning and filtering are handled internally by the receiver firmware. The static rigid-body extrinsic transform between the IMU frame and the GPS antenna frame was determined by mechanical measurement and applied as a fixed parameter during sensor fusion.

5) Data preprocessing

Given embedded filtering on both devices, external preprocessing is minimal and limited to unit normalization, frame alignment, and conservative outlier rejection based on covariance/innovation thresholds.

6) Computational cost analysis

With a modest state dimension and low-dimensional measurements, the runtime is dominated by the small matrix inversion in the update step. The combination of tuned $\mathbf{Q}/\mathbf{R}$ and minimal preprocessing enables real-time execution on a low-cost embedded processor.

III. Results and Discussions

The data collection and processing using GPS, IMU, and odometry sensors were collected at various velocity levels (1 to 5) with three repetitions to ensure the reliability along a 67-meter path. The parameters recorded included position, velocity, acceleration, and orientation. The raw data was extracted into CSV files and processed using Kalman Filter (KF) and Extended Kalman Filters (EKF) to reduce noise and improve accuracy. The processed data was then analyzed to identify patterns, validate consistency, and the performance was compared across different velocities, providing insights into the PMV's behavior and navigation system effectiveness.

Table 4.
Variable used for KF and EKF.

Methods	Variable used		
	GPS	**IMU**	**Odometry**
Kalman Filter	Latitude	Linear acceleration x	
	Longitude	Linear acceleration y	
Extended Kalman Filter	Latitude	Orientation x	Velocity linear x
	Longitude	Orientation y	
	Altitude	Orientation z	
		Orientation w	
		Angular velocity z	

The data in Table 4 represent the variables used for sensor fusion. The KF, designed for linear systems, does not incorporate data from odometry sensors. It processes GPS data by converting latitude and longitude to UTM (Universal Transverse Mercator) coordinates, which use meters and represent the Earth's surface in a nearly flat plane to closely approximate real-world distances. The EKF processes IMU data by converting quaternion orientation data (x, y, z, w) into Euler angles to yield a heading value. Incorporating this heading enhances the accuracy of state estimation, particularly in applications demanding precise orientation information.

In this experiment, the KF and EKF were implemented using the Python programming language. The following figures compare the estimated PMV position generated by each filter against GPS measurements and the actual trajectory. Figure 7 shows the comparison of PMV position generated by KF and EKF, respectively, for velocity 1 (i.e., 0.5 m/s). In each subfigure, the red line represents the actual trajectory, the yellow line shows the raw GPS measurement, the blue line is the estimated path from the KF, and the green line is the estimated path from the EKF.

Figure 7(a), experiment 1, shows that the KF estimate (blue) shows little improvement over the noisy GPS data (yellow). In contrast, the EKF estimate (green) is noticeably smoother, a result of its ability to incorporate and fuse more sensor variables, including orientation.

In Figure 7(b), experiment 2, the estimated state of KF appears smoother compared to experiment 1, and the EKF performance remains consistent. Figure 7(c) represents experiment 3, the KF performance degrades slightly but remains better than in experiment 1. The EKF continues to provide a stable and smooth estimate. The variability in KF performance across these three runs at the same velocity suggests underlying data inconsistencies.

Figure 8 shows a comparison of estimated PMV localization between KF and EKF based on the experiment results for velocity 2 (i.e., 0.7 m/s). Across all three experiments, the EKF estimate (green) consistently produces a smoother path that more closely follows the actual trajectory (red) compared to the KF estimate (blue). The gap between the GPS measurement (yellow) and the KF output is notably larger than the gap for the EKF, highlighting the EKF's superior fusion capabilities.

Figure 9 illustrates the results for velocity 3 (i.e., 0.9 m/s). In Experiment 1, a significant disconnection is observed between the GPS measurement and the KF estimate. The KF performance improves in Experiments 2 and 3. The EKF, however, demonstrates robust and smooth estimation across all three experiments, effectively correlating the GPS data with other sensor inputs to produce a reliable path.

The experimental results at velocity 4 (i.e., 1.0 m/s), shown in Figure 10, highlight a significant discrepancy between the GPS measurements and the KF estimate in Experiments 1 and 2 (Figures 10(a) and 10(b)). The results of experiment 3 (Figure 10(c)) is more favorable for the KF. The EKF approach (Figures 10(a), 10(b), and 10(c)) demonstrates a consistent and notable improvement in tracking the actual trajectory across all three experiments, again proving its effectiveness.

The results of the experiment at velocity 5 (i.e., 1.23 m/s) are shown in Figure 11. The KF results show a large gap in Experiment 3, larger than in the previous two. The EKF, in contrast, provides consistent and accurate estimation results across all three experiments. Analyzing all position graphs confirms that the EKF method significantly enhances GPS positioning accuracy, especially at higher velocities.

Table 5 quantifies the deviations across experiments. At velocities 2–5, the results show a consistent pattern in maximum deviations, with the Extended Kalman Filter (EKF) significantly reducing deviations compared to the global positioning system (GPS) and the Kalman Filter (KF). This aligns with findings in the literature, where EKF-based fusion is established as a superior method for integrating noisy sensor data to achieve robust localization.

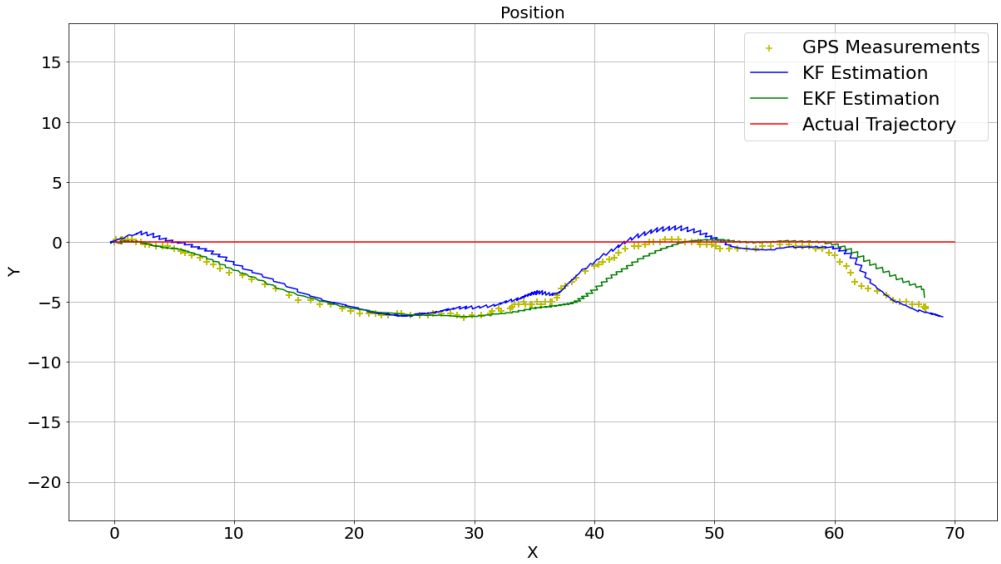

(a)

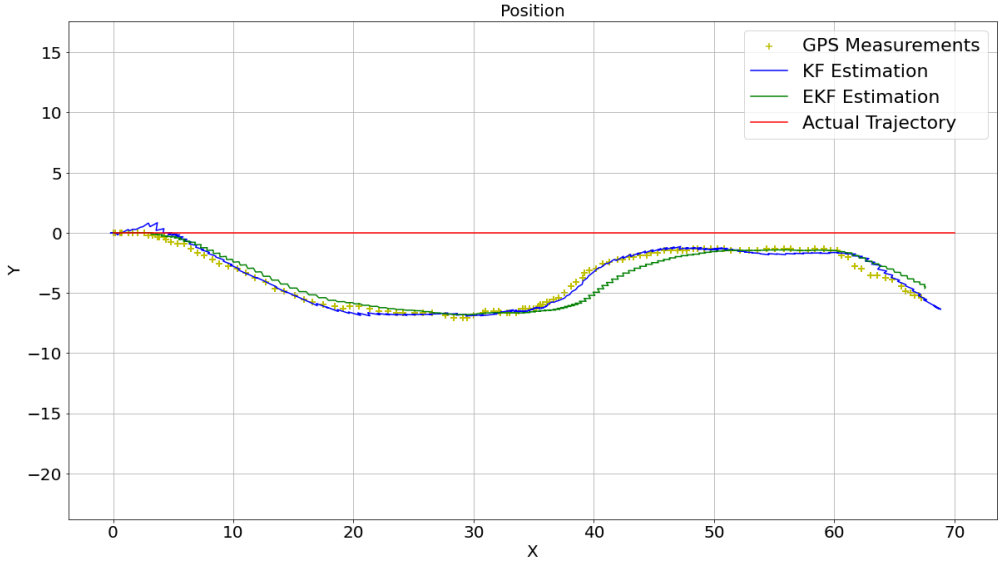

(b)

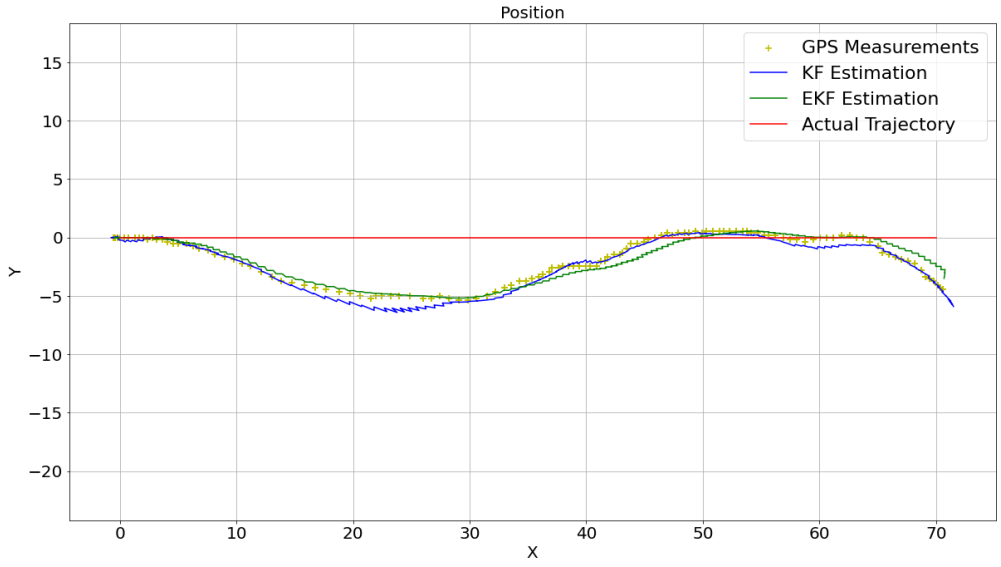

(c)

Figure 7. Position estimation comparison for velocity 1 (i.e., 0.5 m/s). The red line is the actual path, the yellow line is the raw GPS measurement, the blue line is the Kalman Filter (KF) estimate, and the green line is the Extended Kalman Filter (EKF) estimate. (a) data from experiment 1; (b) data from experiment 2; (c) data from experiment 3.

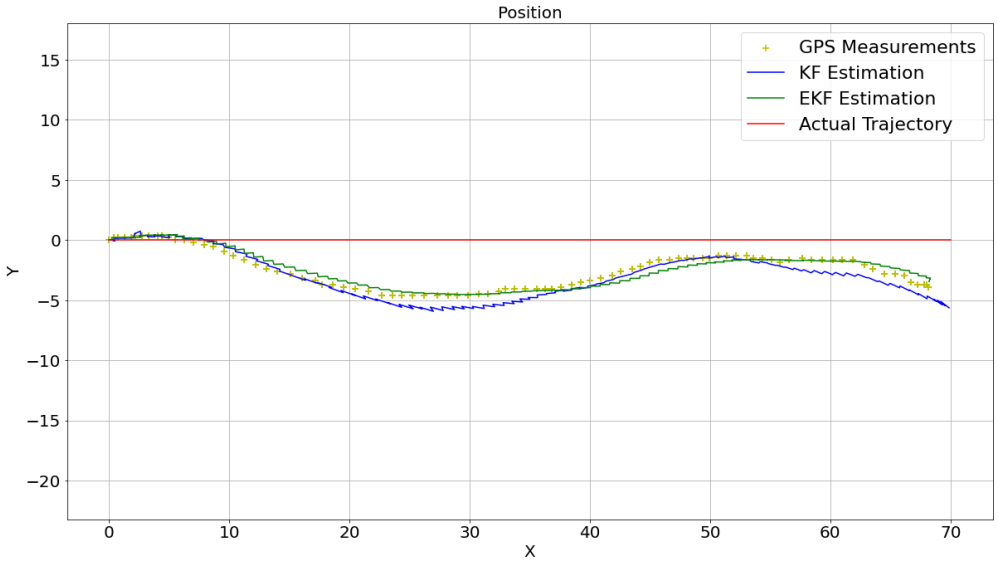

(a)

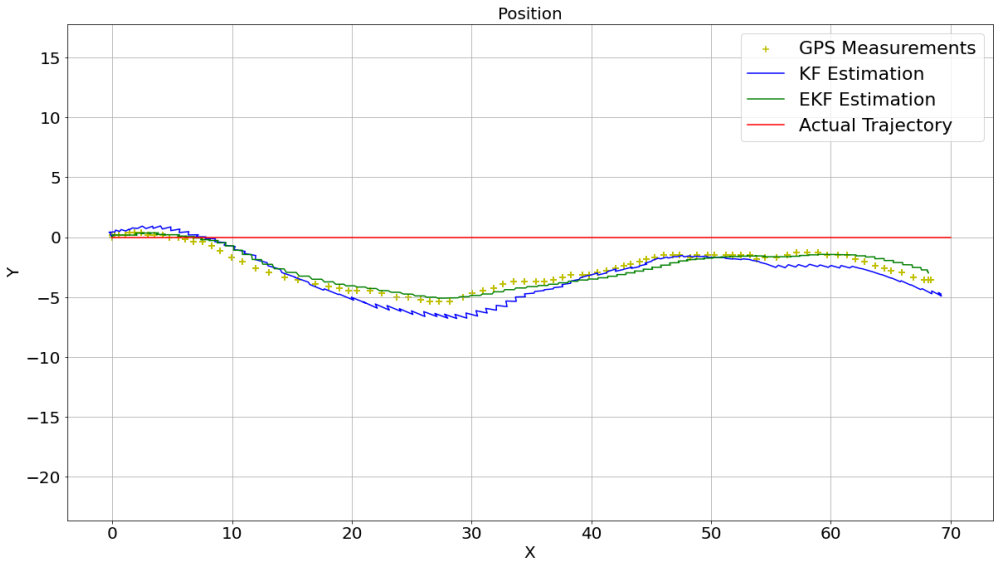

(b)

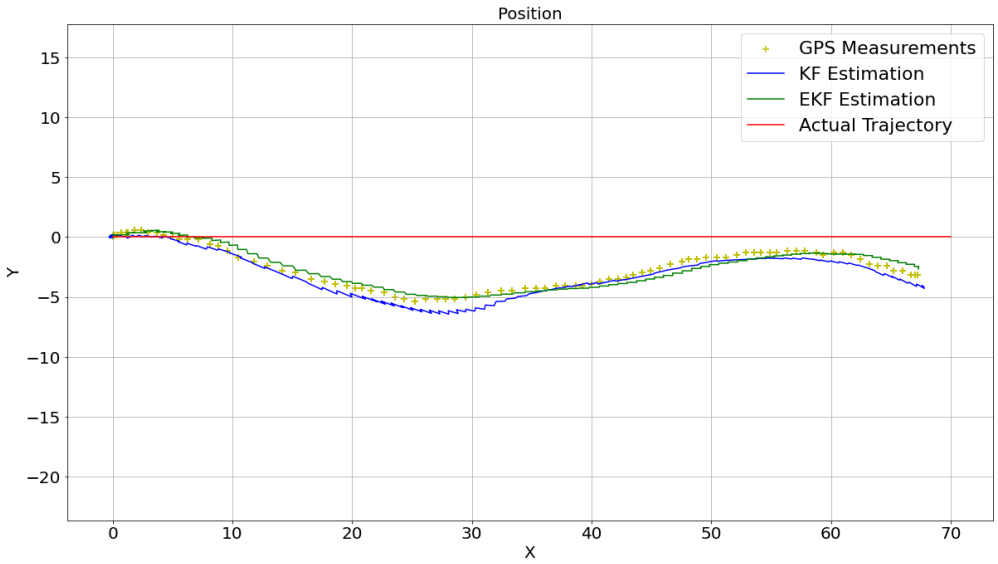

(c)

Figure 8. Position estimation comparison for velocity 2 (i.e., 0.7 m/s). The red line is the actual path, the yellow line is the raw GPS measurement, the blue line is the Kalman Filter (KF) estimate, and the green line is the Extended Kalman Filter (EKF) estimate. (a) data from experiment 1; (b) data from experiment 2; (c) data from experiment 3.

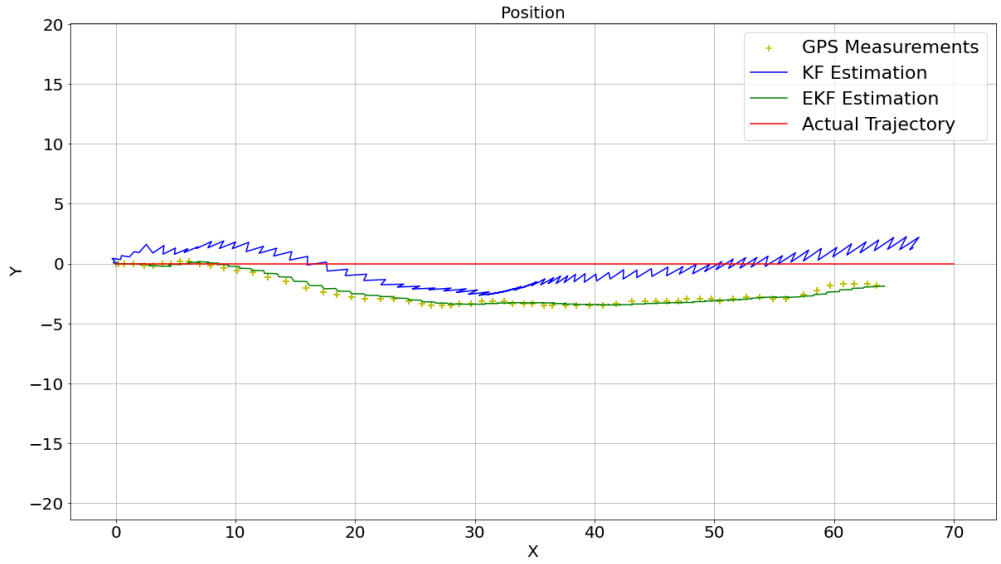

(a)

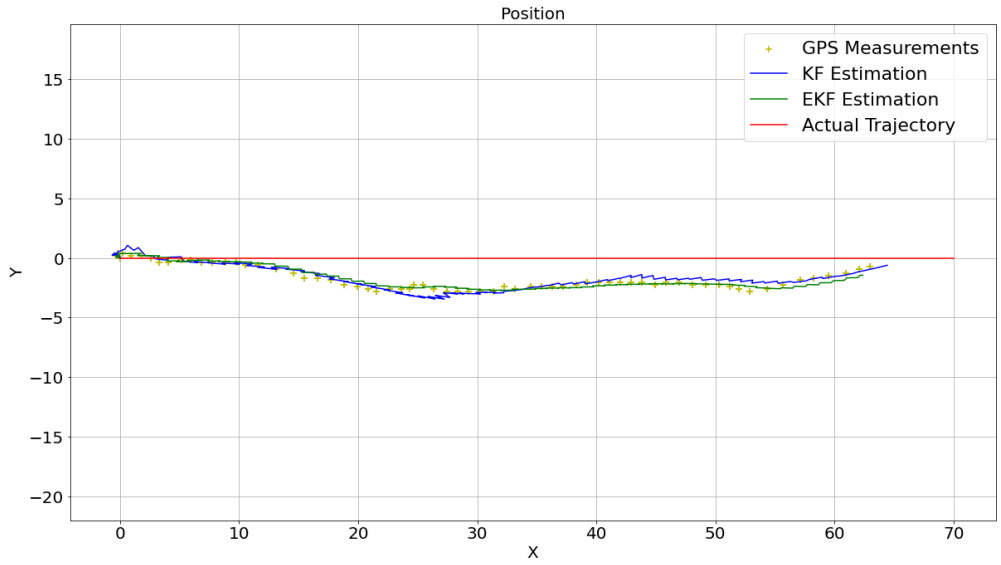

(b)

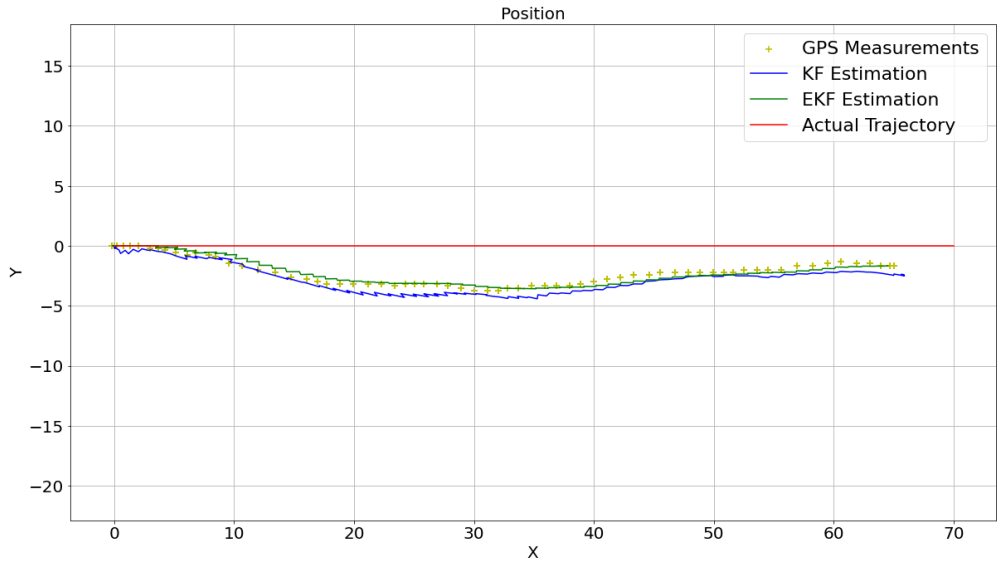

(c)

Figure 9. Position estimation comparison for velocity 3 (i.e., 0.9 m/s). The red line is the actual path, the yellow line is the raw GPS measurement, the blue line is the Kalman Filter (KF) estimate, and the green line is the Extended Kalman Filter (EKF) estimate. (a) data from experiment 1; (b) data from experiment 2; (c) data from experiment 3.

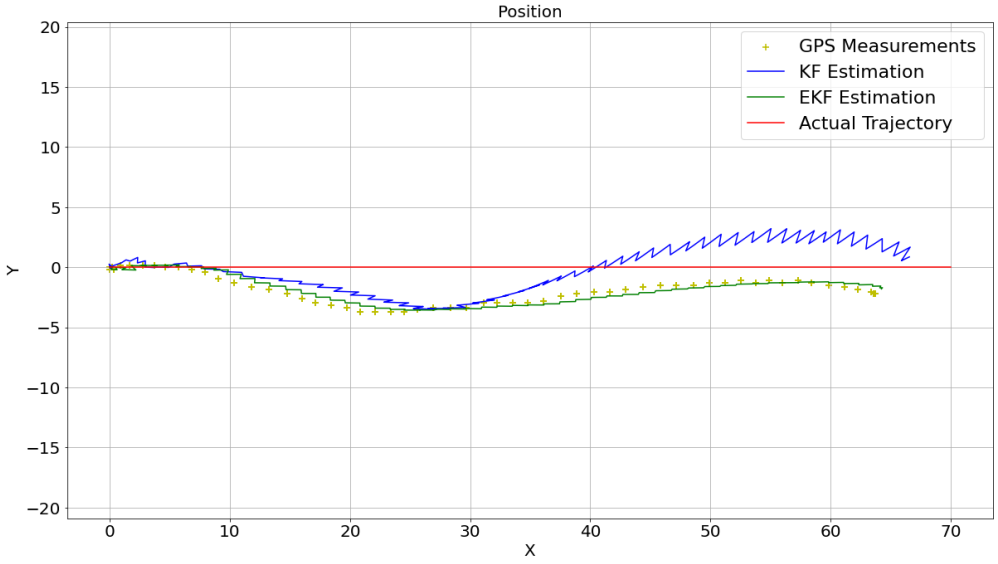

(a)

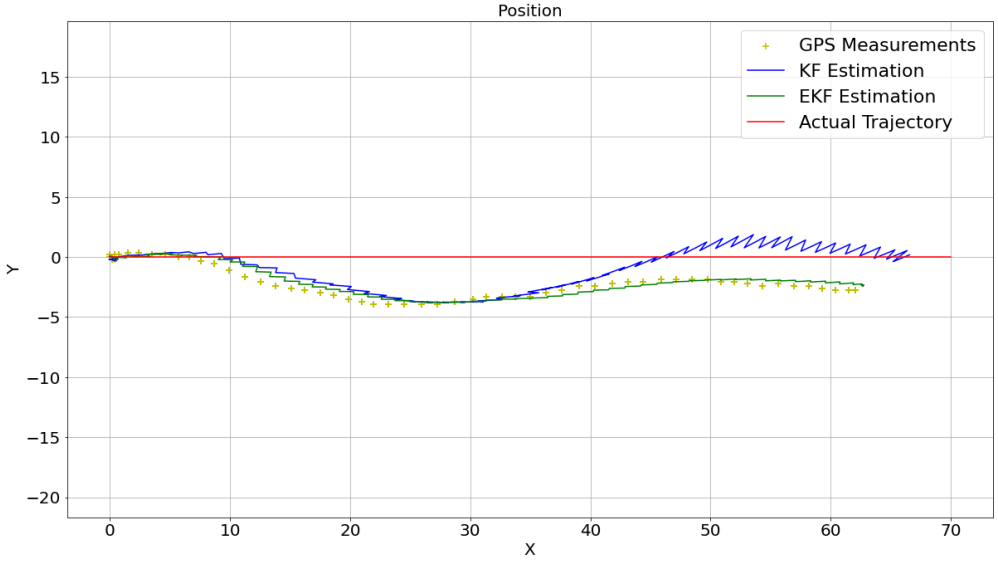

(b)

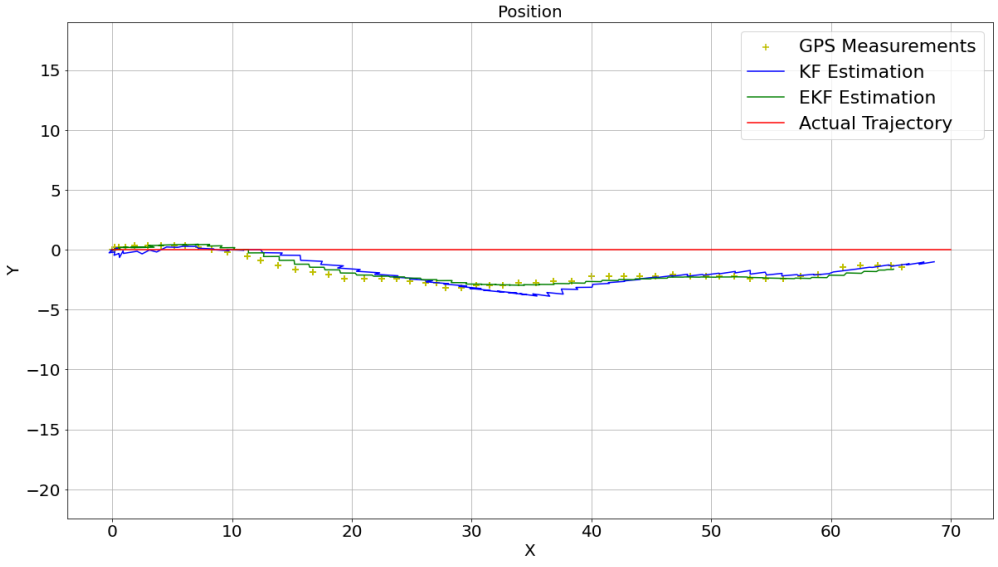

(c)

Figure 10. Position estimation comparison for velocity 4 (i.e., 1.0 m/s). The red line is the actual path, the yellow line is the raw GPS measurement, the blue line is the Kalman Filter (KF) estimate, and the green line is the Extended Kalman Filter (EKF) estimate. (a) data from experiment 1; (b) data from experiment 2; (c) data from experiment 3.

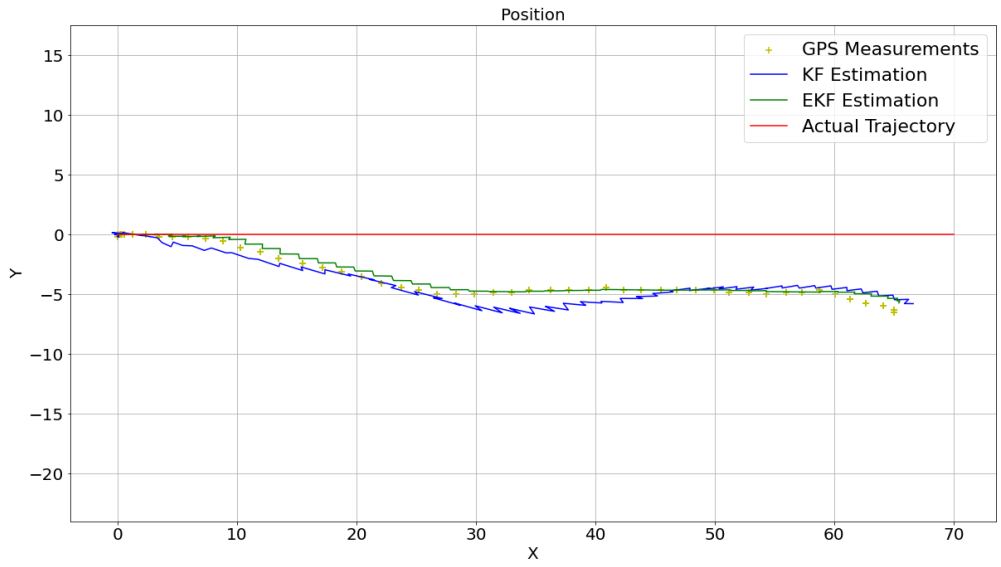

(a)

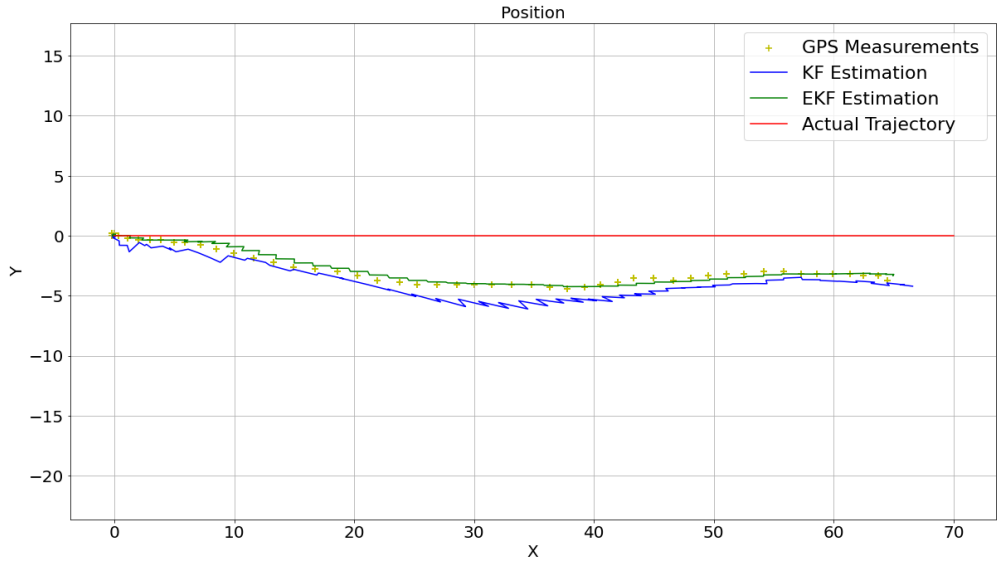

(b)

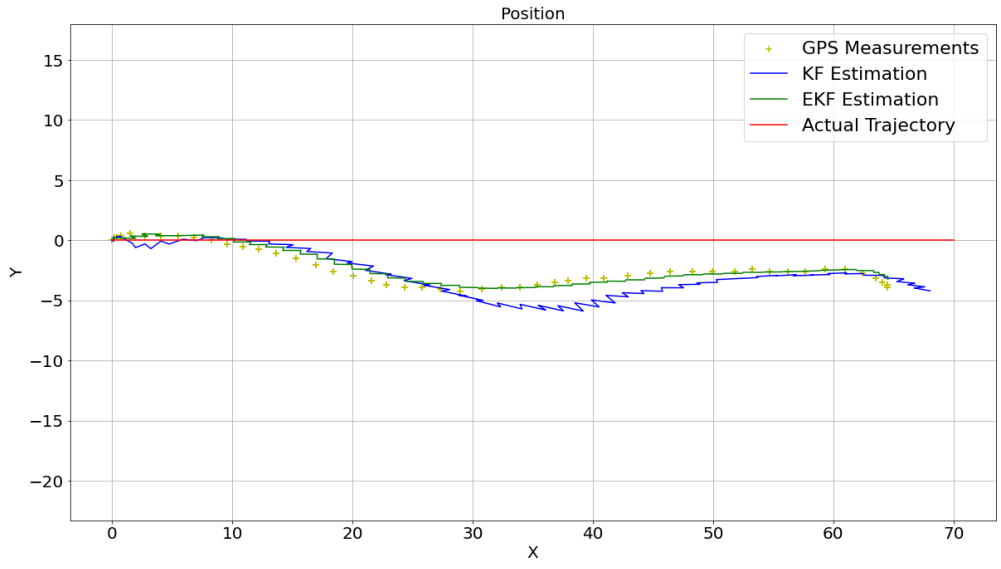

(c)

Figure 11. Position estimation comparison for velocity 5 (i.e., 1.23 m/s). The red line is the actual path, the yellow line is the raw GPS measurement, the blue line is the Kalman Filter (KF) estimate, and the green line is the Extended Kalman Filter (EKF) estimate. (a) data from experiment 1; (b) data from experiment 2; (c) data from experiment 3.

Table 5.
The comparison of the maximum deviation for each experiment.

Experiment		Actual angle	Max. dev (meters)	Standard dev. (meters)
Velocity 1 Exp 1	GPS	-0.082147205	4.441220879	2.791466349
	KF		4.374593162	2.723305061
	EKF		4.900244650	2.959690800
Velocity 1 Exp 2	GPS	-0.079849065	4.792756410	2.716674981
	KF		4.895189691	2.652861422
	EKF		4.539480327	2.648906804
Velocity 1 Exp 3	GPS	-0.063037491	4.138879184	2.476751397
	KF		3.922460401	2.393352093
	EKF		4.092495831	2.479428884
Velocity 2 Exp 1	GPS	-0.057103325	3.343774931	1.634985730
	KF		3.440080683	1.584620518
	EKF		2.958607580	1.548663503
Velocity 2 Exp 2	GPS	-0.051540529	4.012807186	1.688056773
	KF		4.125835309	1.644807493
	EKF		3.688686857	1.659473314
Velocity 2 Exp 3	GPS	-0.046880931	4.197395417	1.755804794
	KF		4.303153379	1.719755914
	EKF		3.717174256	1.696013143
Velocity 3 Exp 1	GPS	-0.029186403	2.756307334	1.059060606
	KF		2.879268504	1.094573606
	EKF		1.907657645	0.612034186
Velocity 3 Exp 2	GPS	-0.011779022	2.529552660	0.934130422
	KF		2.630449147	0.988442003
	EKF		2.343440987	0.895583181
Velocity 3 Exp 3	GPS	-0.025672189	2.940068455	1.088233316
	KF		3.081846533	1.087137655
	EKF		2.709623003	1.023161859
Velocity 4 Exp 1	GPS	-0.034917494	2.984179246	1.167422802
	KF		3.075568334	1.143269313
	EKF		2.710417307	1.138494660
Velocity 4 Exp 2	GPS	-0.044800685	2.913691625	1.053502319
	KF		3.010538711	1.056807862
	EKF		2.594546528	1.030643036
Velocity 4 Exp 3	GPS	-0.022504571	2.528435608	0.946894269
	KF		2.661341913	0.982900310
	EKF		2.207299202	0.905092160
Velocity 5 Exp 1	GPS	-0.099544535	2.341917358	0.897856725
	KF		2.459126889	0.876388158
	EKF		1.852820316	0.870005917
Velocity 5 Exp 2	GPS	-0.057496743	2.629780872	1.008435589
	KF		2.743251058	1.005977777
	EKF		2.343281522	0.941865189
Velocity 5 Exp 3	GPS	-0.060365371	2.519603607	1.084482795
	KF		2.652454142	1.069278176
	EKF		2.178411405	1.034850406

However, the results at velocity 1 (i.e., 0.5 m/s) exhibit an anomalous pattern, where the EKF does not consistently outperform the KF. This anomaly is due to a combination of factors related to low velocity operation. At very low speeds (velocity 1), the PMV's torque may have been insufficient for smooth operation, potentially causing jerky movements that are challenging for the sensor suite to accurately capture. Furthermore, consumer-grade IMUs are poor at estimating orientation at near-zero velocities, as they rely on detecting changes in acceleration. This could have led to erroneous heading data being fed into the EKF, degrading its performance instead of enhancing it. This finding suggests that velocity 1 may fall below the operational threshold for reliable data collection with this specific sensor configuration.

The overall experimental results show that the KF and EKF methods produced less satisfactory outcomes at velocities 1 and 2, likely due to insufficient torque affecting sensor performance. This limitation led to significant discrepancies in GPS positions, as the IMU sensor failed to adequately correct GPS errors. At

velocities 3–5, the EKF approach demonstrated a clear improvement in accuracy. By continuously refining state estimates with updated sensor data, computing Kalman gain, and minimizing the influence of noise, the EKF effectively reduced deviations and improved position estimates. This process ensured that the final state estimations closely matched the true trajectory, enhancing the overall precision and reliability of the navigation system [33].

The results also demonstrate that sensor fusion (i.e., EKF-based fusion) significantly improves localization accuracy by combining data from multiple sensors, including GPS, IMU, and odometry, to overcome the limitations of individual sensors, such as GPS signal degradation or IMU drift [23][34]. This is particularly crucial when using low-cost, consumer-grade sensors, as in this study. While affordable, these sensors have well-documented limitations, including lower precision and higher inherent noise, all of which can affect the overall accuracy and reliability of the system [35][36].

These limitations directly impacted the results. The presence of tall buildings around the test site introduced multipath effects, causing significant GPS inaccuracies [7][24]. The consumer-grade IMU likely experienced considerable drift and noise, especially at lower velocities. The unexpected patterns and inconsistencies observed, particularly the anomalous performance at velocity 1 and the varying performance of the KF across repeated trials at the same velocity, can be attributed to these sensor quality issues and challenging environmental factors.

The implementation of EKF's primary objective is to mitigate these issues by fusing the imperfect data streams. Its superior performance at most velocities demonstrates that while sensor fusion cannot completely eliminate the constraints of low-cost hardware, it is an effective strategy for maximizing their potential and achieving a more accurate and reliable localization solution [24][37][38]. Future work would benefit from testing with higher-grade sensors to establish a performance baseline and further quantify the improvement achievable through fusion algorithms.

IV. Conclusion

This study aimed to enhance the localization accuracy and reliability of PMV in challenging outdoor environments by fusing data from consumer-grade GPS, wheel odometry, and IMU sensors, using Kalman Filter (KF) and Extended Kalman Filter (EKF) methods. The experimental results show that the EKF consistently outperforms the standard KF, particularly at medium to higher velocities (3–5), where EKF enhances vehicle position accuracy by approximately 29 %, and reduces the maximum deviation to a range of 1.8 m to 2.7 m. EKF-based sensor fusion demonstrates significant potential. However, the study also revealed notable limitations. Performance was notably weaker at lower velocities (1–2), where anomalies suggested that insufficient torque and the inherent limitations of consumer-grade IMUs in estimating orientation at near-zero speeds degraded sensor fusion performance. Furthermore, multipath effects from nearby tall buildings introduced substantial GPS noise, highlighting the vulnerability of relying on consumer-grade GNSS in urban canyons. For future work, several aspects for improvement are recommended. First, with advancements in sensor technology and cost reductions, incorporating additional sensors like LiDAR and cameras could provide complementary data for scan matching and visual odometry, drastically reducing dependence on error-prone GPS signals, and can further improve navigation system precision and reliability. Second, exploring advanced algorithms like Unscented Kalman Filters (UKF) or AI-driven deep sensor fusion networks could better handle the non-linearities and complex noise characteristics of low-cost sensors. For real-world deployment, scaling this system presents challenges, including the computational load of processing data from multiple high-frequency sensors on embedded hardware. Incorporating more advanced computational methods is expected to enhance the efficiency and performance of EKF-based systems. Moreover, robust calibration procedures across diverse operating conditions and ensuring system resilience against unpredictable environmental factors are also essential for making them suitable for a wide range of applications, from personal mobility vehicles to large-scale autonomous transportation networks.

Acknowledgements

This work is supported by a research project funded by the Research Organization for Electronics and Informatics, National Research and Innovation Agency (BRIN). The author would also like to thank the UTM lecturers, BRIN researchers, and research assistants who helped in the accomplishment of this work.

Declarations

Author contribution

V. Susanti, M.S.A. Mahmud, and R.P. Saputra contributed equally as the main contributor of this paper. All authors read and approved the final paper.

Funding statement

This research did not receive any specific grant from funding agencies in the public, commercial, or not-for-profit sectors.

Competing interest

The authors declare no conflict of interest.

Additional information

Reprints and permission: information is available at https://mev.brin.go.id/.

Publisher's Note: National Research and Innovation Agency (BRIN) remains neutral with regard to jurisdictional claims in published maps and institutional affiliations.

References

[1] S. Akter, M. M. H. Mamun, J. L. Mwakalonge, G. Comert, and S. Siuhi, "A policy review of electric personal assistive mobility devices," *Transp. Res. Interdiscip. Perspect.*, vol. 11, no. March, p. 100426, 2021.

[2] C. W. Pyo, H. Sawada, and T. Matsumura, "Experimental study of dynamic data traffic control for the cooperating system of smart personal mobility and indoor intelligent infrastructure," *Int. Symp. Wirel. Pers. Multimed. Commun. WPMC*, vol. 2021-Decem, pp. 1–6, 2021.

[3] K. Maeda and S. Nakajima, "Human machine interface to provide a driver with information on a next motion of personal mobility vehicles," *2021 60th Annu. Conf. Soc. Instrum. Control Eng. Japan, SICE 2021*, pp. 1227–1232, 2021.

[4] M. Jayasuriya, G. Dissanayake, R. Ranasinghe, and N. Gandhi, "Leveraging deep learning based object detection for localising autonomous personal mobility devices in sparse maps," *2019 IEEE Intell. Transp. Syst. Conf. ITSC 2019*, pp. 4081–4086, 2019.

[5] Z. Yu, Y. Hu, and J. Huang, "GPS/INS/Odometer/DR integrated navigation system aided with vehicular dynamic characteristics for autonomous vehicle application," *IFAC-PapersOnLine*, vol. 51, no. 31, pp. 936–942, 2018.

[6] R. Ross and R. Hoque, "Augmenting GPS with geolocated fiducials to improve accuracy for mobile robot applications," *Appl. Sci.*, vol. 10, no. 1, 2020.

[7] T. Aydin and E. Erdem, "Novel deep hybrid and ensemble algorithms for improving GPS navigation positioning accuracy," *IEEE Access*, vol. 11, no. May, pp. 53518–53530, 2023.

[8] S. Y. Alaba, "GPS-IMU sensor fusion for reliable autonomous vehicle position estimation," *arXiv.org*, 2024, [Online].

[9] T. Ngoc Huy, L. Manh Cam, and N. Thanh Nam, "GPS/INS integrated navigation system for autonomous robots," *Sci. Technol. Dev. J. - Eng. Technol.*, vol. 3, no. SI1, p. First, Apr. 2020.

[10] J. Cheng, L. Zhang, Q. Chen, X. Hu, and J. Cai, "Map aided visual-inertial fusion localization method for autonomous driving vehicles," *Meas. J. Int. Meas. Confed.*, vol. 221, no. September 2021, p. 113432, 2023.

[11] M. Khosyi'in, S. A. D. Prasetyowati, Z. Nawawi, and B. Y. Suprapto, "Review and design of GPS-RFID localization for autonomous vehicle navigation," *ACM International Conference Proceeding Series*. pp. 42–46, 2019.

[12] K. Baxevani, I. Yadav, Y. Yang, M. Sebok, H. G. Tanner, and G. Huang, "Resilient ground vehicle autonomous navigation in GPS-denied environments," *Guid. Navig. Control*, vol. 2, no. 4, pp. 1–17, 2022.

[13] A. Thakur and S. K. Mishra, "An in-depth evaluation of deep learning-enabled adaptive approaches for detecting obstacles using sensor-fused data in autonomous vehicles," *Eng. Appl. Artif. Intell.*, vol. 133, no. PF, p. 108550, 2024.

[14] X. Shan, A. Cabani, and H. Chafouk, "Cooperative localization based on GPS correction and EKF in urban environment," *2022 2nd Int. Conf. Innov. Res. Appl. Sci. Eng. Technol. IRASET 2022*, pp. 1–8, 2022.

[15] B. Dahmane, B. Lejdel, E. Clementini, F. Harrats, S. Nassar, and L. H. Abderrahmane, "Controlling the degree of observability in GPS/INS integration land-vehicle navigation based on extended kalman filter," *Bull. Electr. Eng. Informatics*, vol. 11, no. 2, pp. 702–712, 2022.

[16] N. Allan Anbu and D. Jayaprasanth, "Integration of inertial navigation system with global positioning system using Extended Kalman Filter," *Proc. 2nd Int. Conf. Smart Syst. Inven. Technol. ICSSIT 2019*, no. Icssit, pp. 789–794, 2019.

[17] K. Kumar, S. Bhaumik, and P. Date, "Extended Kalman Filter using orthogonal polynomials," *IEEE Access*, vol. 9, pp. 59675–59691, 2021.

[18] H. Zhang, X. Zhang, W. Xie, and J. Du, "Smoothly constrained Extended Kalman Filter," in *2020 15th IEEE International Conference on Signal Processing (ICSP)*, IEEE, Dec. 2020, pp. 52–55.

[19] Y. Ollivier, "The Extended Kalman Filter is a natural gradient descent in trajectory space," *arXiv.org*, Jan. 2019, [Online].

[20] J. Huang, Y. Lian, J. Wang, B. Dong, and Z. Shi, "Extended Kalman Filter-based vehicle state estimation for direct yaw moment control systems," in *2022 5th International Conference on Robotics, Control and Automation Engineering (RCAE)*, IEEE, Oct. 2022, pp. 6–10.

[21] A. Kaczmarek, W. Rohm, L. Klingbeil, and J. Tchórzewski, "Experimental 2D extended Kalman filter sensor fusion for low-cost GNSS/IMU/Odometers precise positioning system," *Measurement*, vol. 193, 2022.

[22] S. Y. Alaba, "GPS-IMU sensor fusion for reliable autonomous vehicle position estimation," *ArXiv*, 2024, [Online].

[23] V. Girbés-Juan, L. Armesto, D. Hernández-Ferrándiz, J. F. Dols, and A. Sala, "Asynchronous sensor fusion of GPS, IMU and CAN-based odometry for heavy-duty vehicles," *IEEE Trans. Veh. Technol.*, vol. 70, no. 9, pp. 8617–8626, 2021.

[24] C. Shien, C. Huang, J. Liu, X. Chen, U. Weijinya, and G. Shi, "Integrated navigation accuracy improvement algorithm based on multi-sensor fusion," *2019 IEEE The 2nd International Conference On Micro/Nano Sensors for AI, Healthcare, And Robotics (NSENS)*. IEEE, 2019.

[25] J. Zagorskas and M. Burinskiene, "Challenges caused by increased use of E-powered personal mobility vehicles in European cities," *Sustain.*, vol. 12, no. 1, 2020.

[26] Y. Morales, N. Akai, and H. Murase, "Personal mobility vehicle autonomous navigation through pedestrian flow: A data driven approach for parameter extraction," *IEEE Int. Conf. Intell. Robot. Syst.*, pp. 3438–3444, 2018.

[27] S. H. Kim, H. Lim, and J. Kim, "Exploring countermeasures from a psychological perspective to create a safe driving environment for personal mobility devices," *Sustain.*, vol. 13, no. 10, 2021.

[28] T. Hishikawa and M. Iryo-Asano, "Safety evaluation of personal mobility vehicles and pedestrians under mixed traffic flow using traffic simulation," *Asian Transp. Stud.*, vol. 8, no. February, p. 100049, 2022.

[29] R. R. Pratama *et al.*, "Non-linear model predictive control with single-shooting method for autonomous personal mobility vehicle," *J. Mechatronics, Electr. Power, Veh. Technol.*, vol. 15, no. 2, pp. 186–196, 2024.

[30] A. P. Martorell, "Improvement of a positioning system for assisted and autonomous driving," Universitat Politècnica de Catalunya, 2021.

[31] M. H. Gusrial, N. A. Othman, H. Ahmad, and M. H. A. Hassan, "Review of Kalman filter variants for SLAM in mobile robotics with linearization and covariance initialization," *J. Mechatronics, Electr. Power, Veh. Technol.*, vol. 16, no. 1, pp. 69–83, Jul. 2025.

[32] J. Owoyemi, "Kalman Filter: Predict, measure, update, repeat.," 2017. (accessed Mar. 25, 2024).

[33] A. N. Ouda and A. Mohamed, "Hybrid positioning technique based integration of GPS/INS for an autonomous vehicle navigation," *Adv. Mil. Technol.*, vol. 17, no. 2, pp. 357–382, 2022.

[34] B. Suwandi, W. S. Pinastiko, and R. Roestam, "OBD-II sensor approaches for the IMU and GPS based apron vehicle positioning system," *ICSECC 2019 - Int. Conf. Sustain. Eng. Creat. Comput. New Idea, New Innov. Proc.*, pp. 251–254, 2019.

[35] A. Salehabadi, M. Enhessari, M. I. Ahmad, N. Ismail, and B. D. Gupta, "Environmental sensors," *Met. Chalcogenide Biosens.*, pp. 99–120, 2023.

[36] H. Y. Teh, A. W. Kempa-Liehr, and K. I. K. Wang, "Sensor data quality: A systematic review," *J. Big Data*, vol. 7, no. 1, pp. 1–49, 2020.

[37] H. Obeidat, W. Shuaieb, O. Obeidat, and R. Abd-Alhameed, "A review of indoor localization techniques and wireless technologies," *Wireless Pers Commun*, vol. 119, pp. 289-327, 2021.

[38] S. Zekavat *et al.*, "An overview on position location: Past, present, future," Int. J. Wireless Inf. Networks, vol. 28, pp. 45-76, 2021.